Electronic Supplementary Material (ESI) for New Journal of Chemistry.

Supporting Information

Simple Tuning the Luminescence Properties of the Double Rollover Cycloplatinated(II) Structure by Halide Ligands

*Sareh Paziresh,[a] Reza Babadi Aghakhanpour,[b] Mehdi Rashidi [a], S. Masoud Nabavizadeh [a]**

[a]Department of Chemistry, College of Sciences, Shiraz University, Shiraz, 71454, Iran

[b]Department of Chemistry, Institute for Advanced Studies in Basic Sciences (IASBS), Yousef Sobouti Blvd., Zanjan 45137-66731, Iran.

Contents:	**Page**

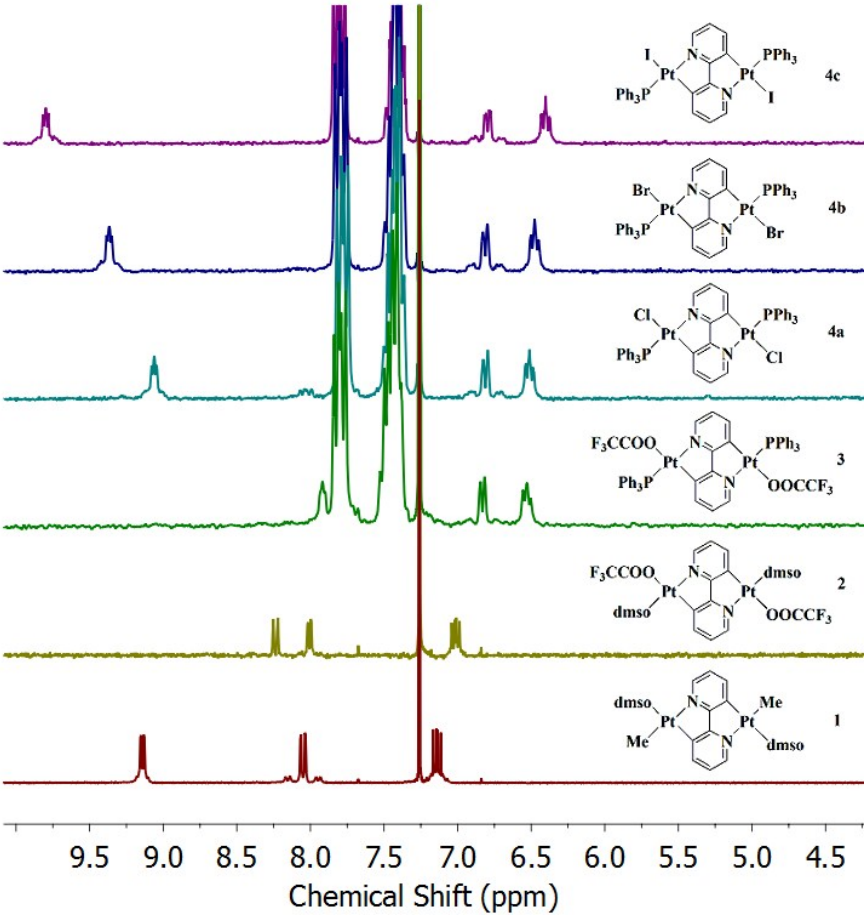

Figure S1. Comparative aromatic regions of the ^{1}H NMR spectra for the complexes **1-3** and **4a-c**.

Table S1. Selected ^{1}HNMR (aromatic regions), ^{31}PNMR spectra chemical shifts δ (ppm) and J_{PtH}, J_{PtP} coupling constant values (Hz) for all the complexes (**1-3**, **4a-c**).

Complex	δH^3	δH^2	δH^1	$^3J_{PtH^3}$	$^3J_{PtH^1}$	δP	$^1J_{PtP}$	Ref.
1	8.05	7.14	9.14	51.6	16.2	-	-	48
2	8.00	7.01	8.24	31.2	25.1	-	-	Present study
3	6.83	6.53	7.93	44.6	26.0	16.87	4230	Present study
4a	6.81	6.51	9.06	47.4	28.9	19.55	4138	Present study and 48
4b	6.82	6.49	9.37	48.0	28.0	18.48	4117	Present study
4c	6.80	6.40	9.80	48.3	28.6	17.66	4065	Present study

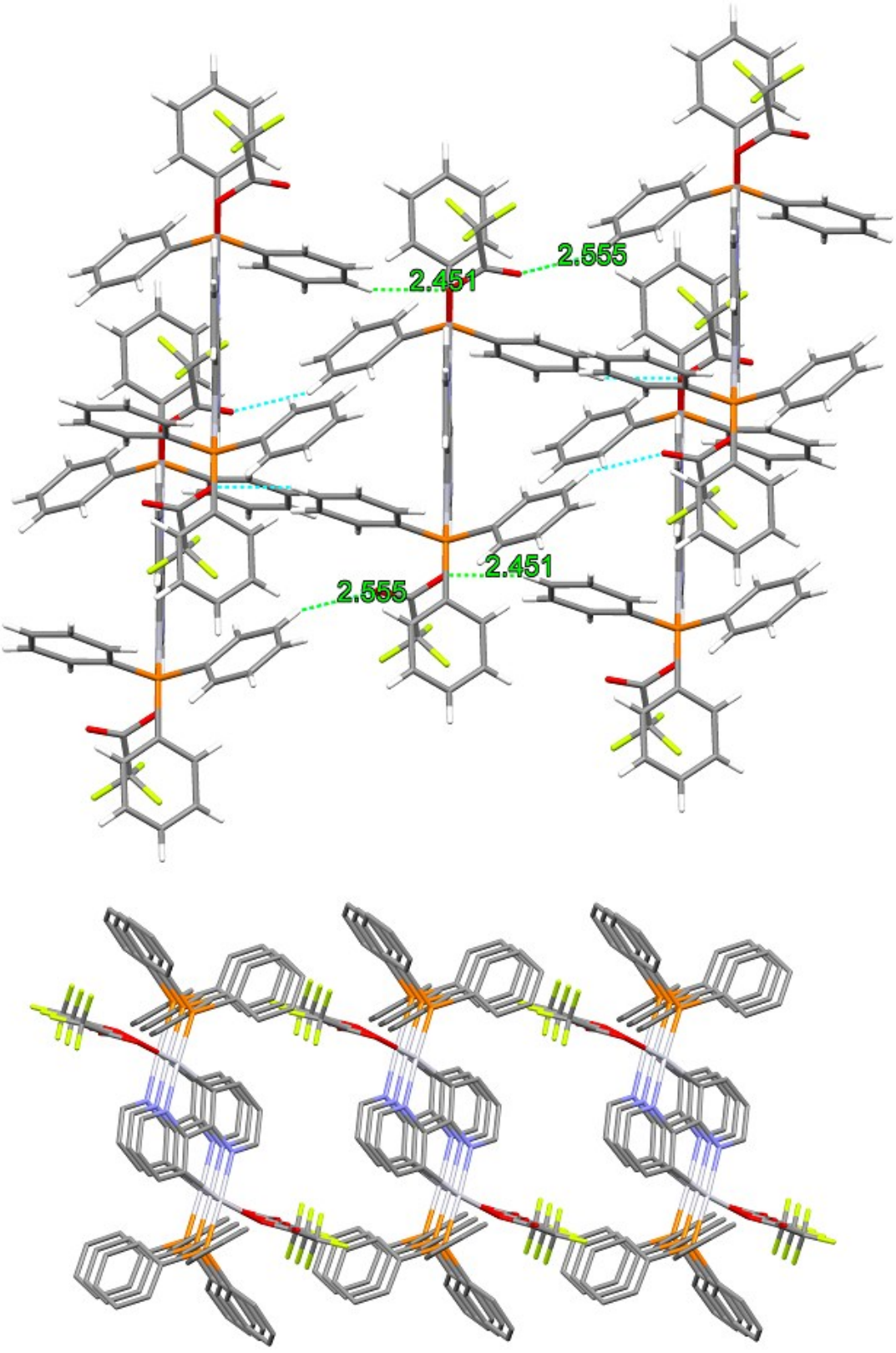

Figure S2. Crystal packing views of the complex **3**.

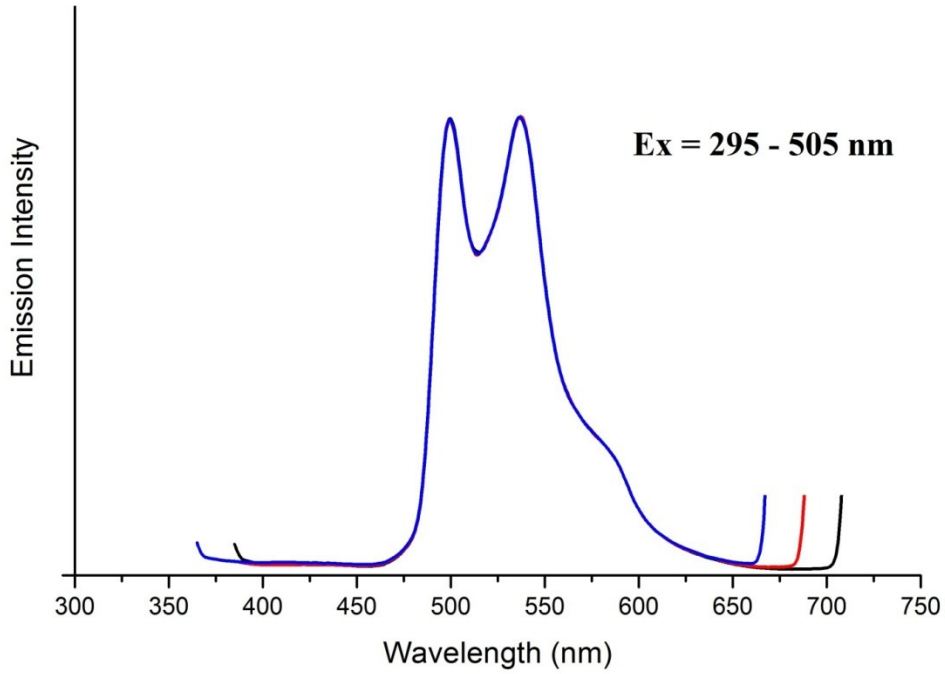

Figure S3. Emission bands for the complex **3** (Excitation wavelength range = 295-505 nm)

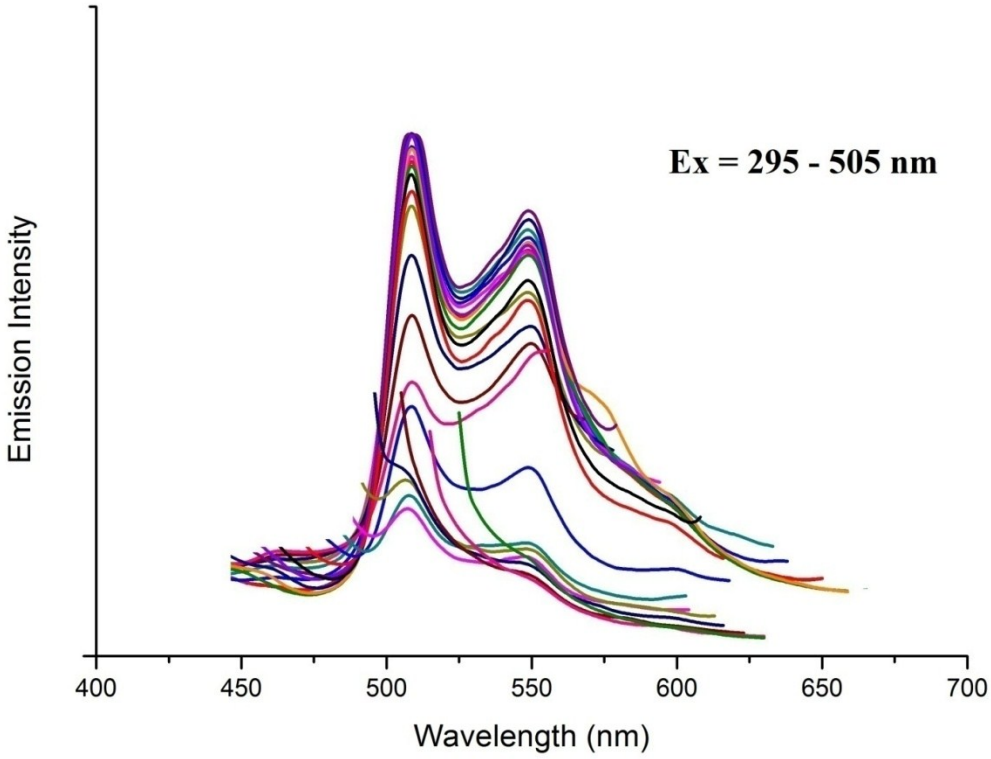

Figure S4. Emission bands for the complex **4a** (Excitation wavelength range = 295-505 nm)

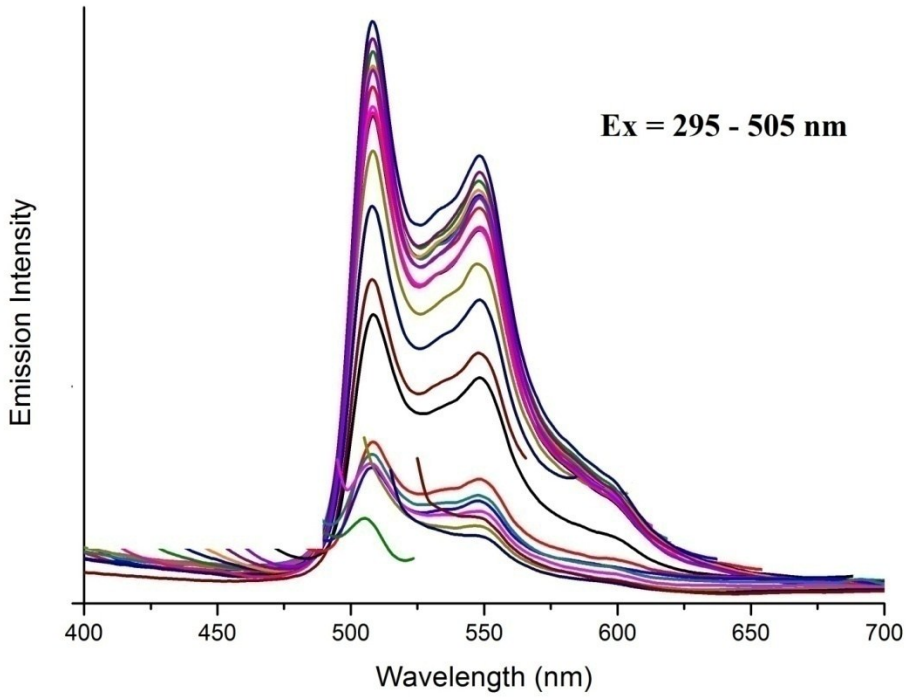

Figure S5. Emission bands for the complex **4b** (Excitation wavelength range = 295-505 nm)

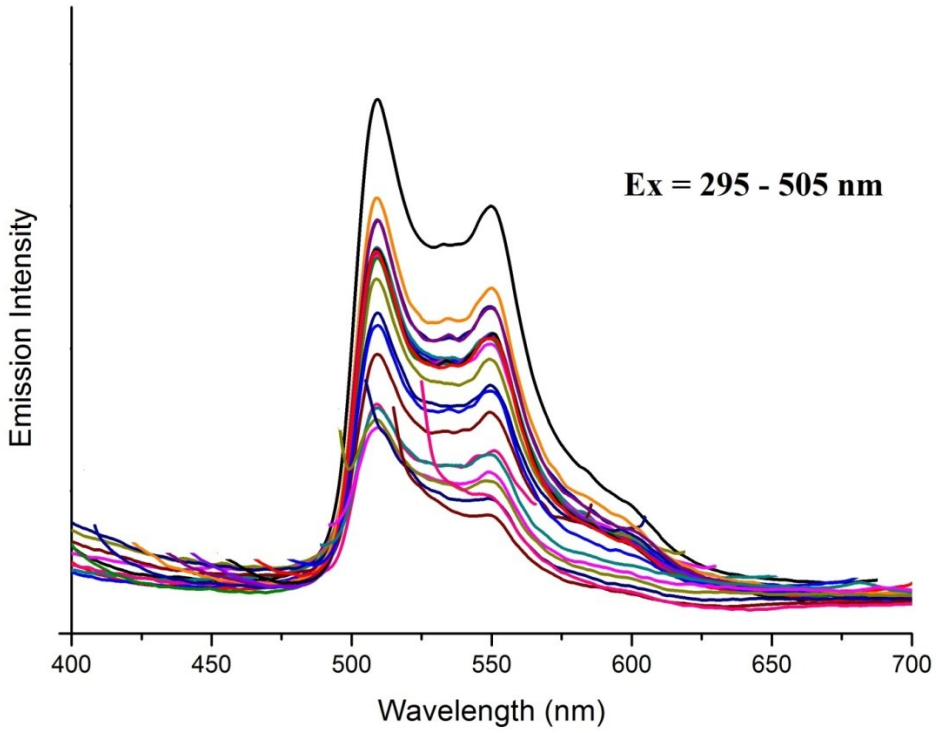

Figure S6. Emission bands for the complex **4c** (Excitation wavelength range = 295-505 nm)

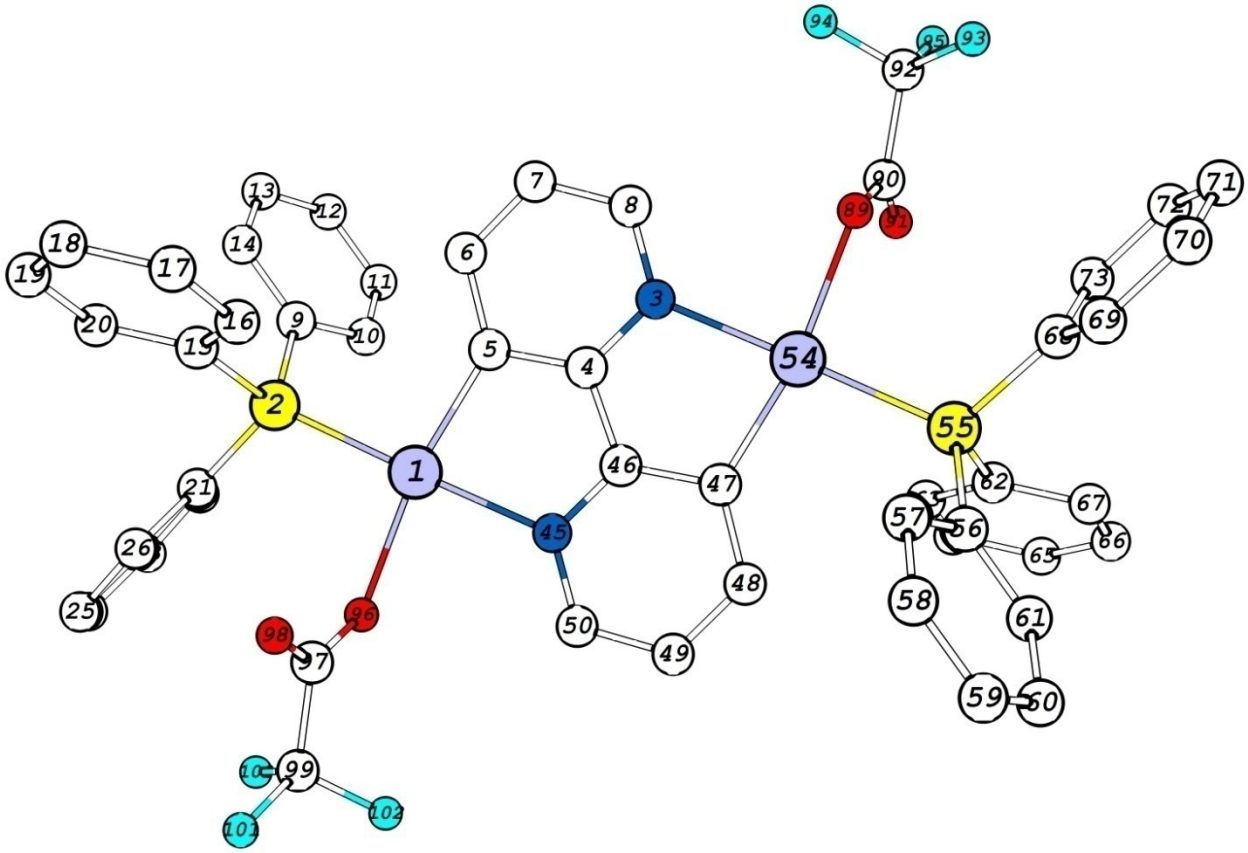

Figure S7. View of the DFT optimized structure of complex $[Pt_2(\mu\text{-bpy-2H})(CF_3COO)_2(PPh_3)_2]$, **3**.

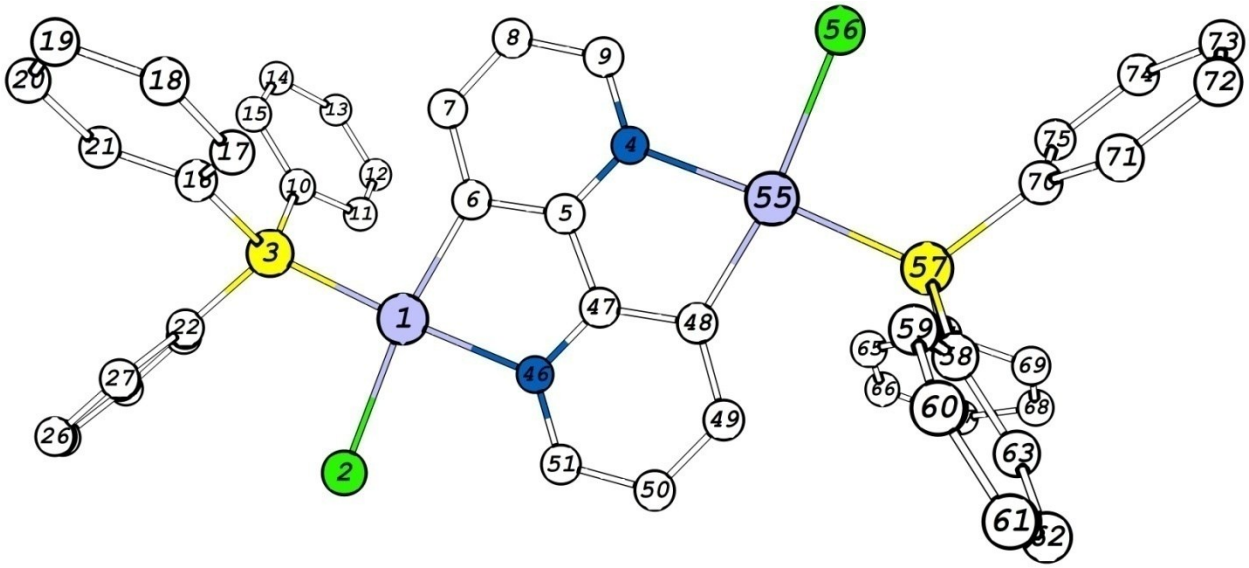

Figure S8. View of the DFT optimized structure of complex $[Pt_2(\mu\text{-bpy-2H})(Cl)_2(PPh_3)_2]$, **4a**.

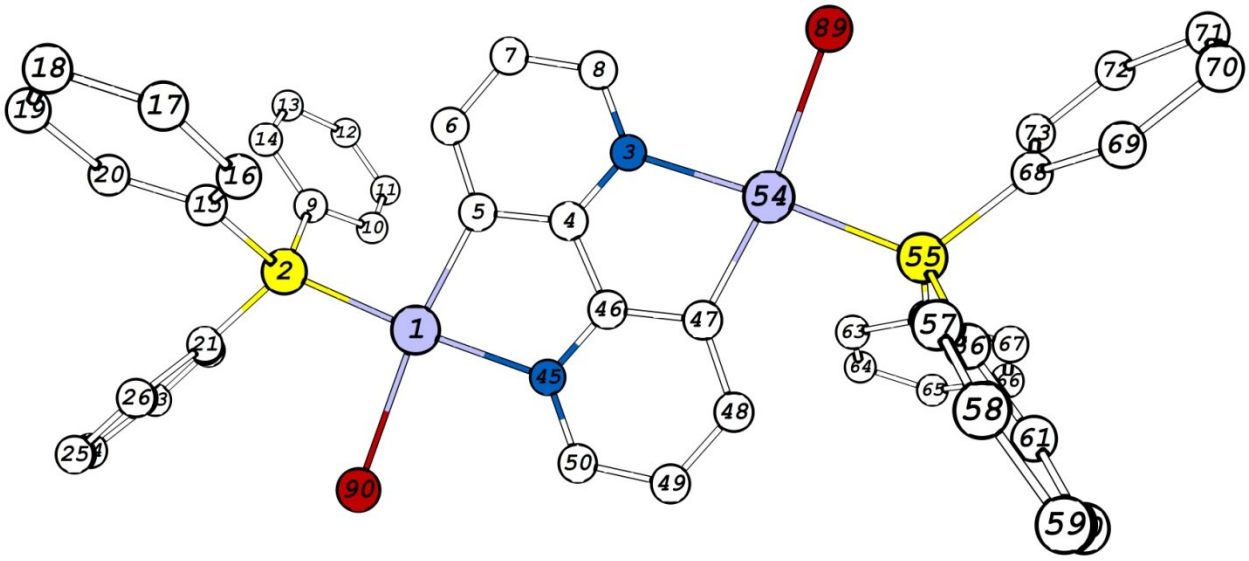

Figure S9. View of the DFT optimized structure of complex $[Pt_2(\mu\text{-bpy-2H})(Br)_2(PPh_3)_2]$, **4b**.

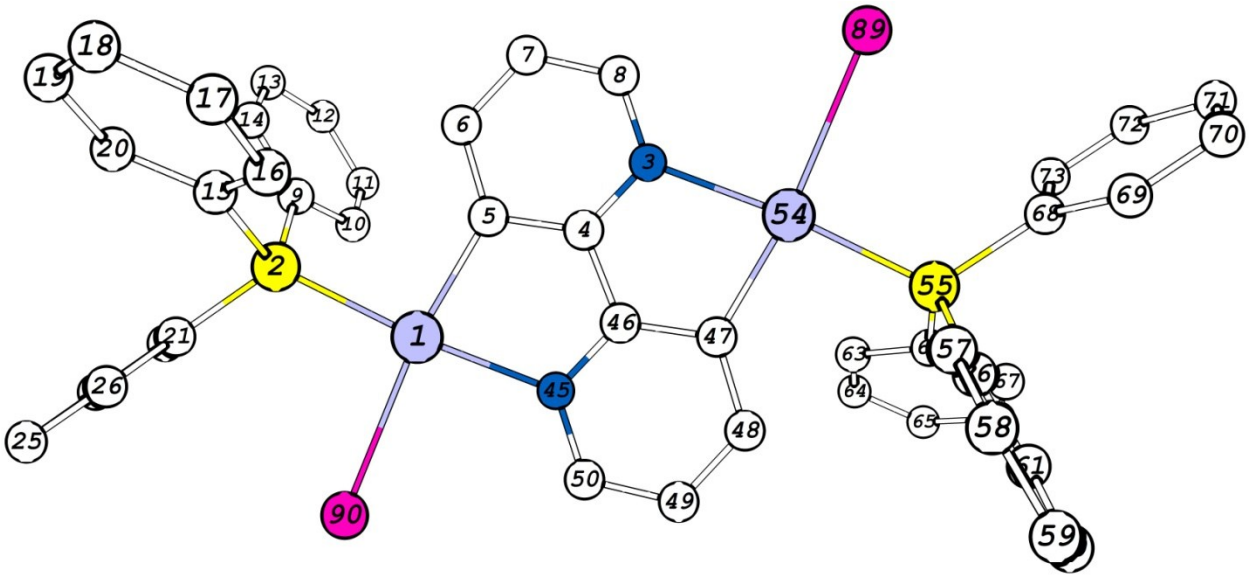

Figure S10. View of the DFT optimized structure of complex $[Pt_2(\mu\text{-bpy-2H})(I)_2(PPh_3)_2]$, **4c**.

Table S2. Selected calculated bond distances (A°) and angles (deg) for the complex [Pt_2(μ-bpy-2H)($CF_3COO)_2$($PPh_3)_2$], **3**, in solid state (S_0 and T_1 states).

Bond distance or angle	S_0	T_1
Pt1-C5	2.027	2.001
Pt1-N45	2.128	2.106
Pt1-P2	2.302	2.315
Pt1-O96	2.135	2.136
O96-C97	1.288	1.288
C97-O98	1.224	1.224
C97-C99	1.552	1.552
C99-F100	1.340	1.340
C99-F101	1.358	1.358
C99-F102	1.348	1.348
P2-C15	1.836	1.836
P2-C21	1.842	1.843
P2-C9	1.846	1.845
N45-C46	1.348	1.399
C46-C4	1.449	1.369
C4-C5	1.408	1.463
N45-Pt1-C5	81.49	82.60
C5-Pt1-P2	97.79	97.58
P2-Pt1-O96	93.37	93.40
O96-Pt1-N45	87.30	86.40
O96-Pt1-C5	168.80	169.01
N45-Pt1-P2	177.42	177.69
Pt1-N45-C46	112.94	111.56
N45-C46-C4	114.53	115.37
C46-C4-C5	119.99	120.53
C4-C5-Pt1	111.02	109.91
O96-C97-O98	129.80	129.77
O96-C97-C99	110.77	119.45

Table S3. Selected calculated bond distances (A°) and angles (deg) for the complex [Pt_2(μ-bpy-2H)$(Cl)_2(PPh_3)_2$], **4a**, in solid state (S_0 and T_1 states).

Bond distance or angle	S_0	T_1
Pt1-C6	2.039	2.012
Pt1-N46	2.142	2.119
Pt1-P3	2.301	2.316
Pt1-Cl2	2.442	2.440
P3-C22	1.842	1.843
P3-C16	1.844	1.844
P3-C10	1.845	1.845
N46-C47	1.351	1.397
C47-C5	1.447	1.370
C5-C6	1.408	1.459
N46-Pt1-C6	80.80	81.94
C6-Pt1-P3	96.49	96.31
P3-Pt1-Cl2	92.26	92.28
Cl2-Pt1-N46	90.43	89.45
Cl2-Pt1-C6	171.24	171.38
N46-Pt1-P3	177.24	178.24
Pt1-N46-C47	113.13	111.74
N46-C47-C5	114.70	115.54
C47-C5-C6	119.77	120.31
C5-C6-Pt1	111.57	110.44

Table S4. Selected calculated bond distances (A°) and angles (deg) for the complex [Pt_2(μ-bpy-2H)$(Br)_2(PPh_3)_2$], **4b**, in solid state (S_0 and T_1 states).

Bond distance or angle	S_0	T_1
Pt1-C5	2.044	2.017
Pt1-N45	2.149	2.126
Pt1-P2	2.304	2.320
Pt1-Br90	2.568	2.566
P2-C21	1.844	1.844
P2-C15	1.844	1.845
P2-C9	1.847	1.846
N45-C46	1.352	1.398
C46-C4	1.447	1.371
C4-C5	1.408	1.458
N45-Pt1-C5	80.53	81.67
C5-Pt1-P2	96.07	95.85
P2-Pt1-Br90	92.23	92.34
Br90-Pt1-N45	91.15	90.12
Br90-Pt1-C5	171.68	171.80
N45-Pt1-P2	176.48	177.45
Pt1-N45-C46	113.16	111.76
N45-C46-C4	114.80	115.66
C46-C4-C5	119.70	120.22
C4-C5-Pt1	111.79	110.66

Table S5. Selected calculated bond distances (A°) and angles (deg) for the complex [Pt_2(μ-bpy-2H)$(I)_2(PPh_3)_2$], **4c**, in solid state (S_0 and T_1 states).

Bond distance or angle	S_0	T_1
Pt1-C5	2.049	2.022
Pt1-N45	2.162	2.137
Pt1-P2	2.309	2.325
Pt1-I90	2.799	2.799
P2-C21	1.845	1.846
P2-C15	1.846	1.846
P2-C9	1.848	1.848
N45-C46	1.354	1.399
C46-C4	1.446	1.371
C4-C5	1.408	1.457
N45-Pt1-C5	80.16	81.31
C5-Pt1-P2	95.01	94.75
P2-Pt1-I90	92.60	92.81
I90-Pt1-N45	92.20	91.12
I90-Pt1-C5	172.36	172.17
N45-Pt1-P2	175.12	176.05
Pt1-N45-C46	113.06	111.67
N45-C46-C4	114.96	115.84
C46-C4-C5	119.58	120.07
C4-C5-Pt1	112.21	111.08

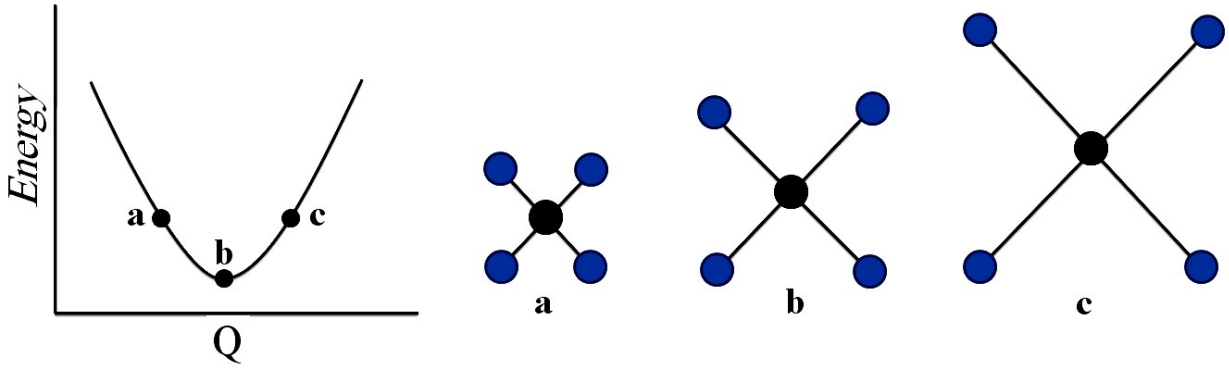

Figure S11. The potential energy of a symmetric breathing vibration.

Table S6. The energies of the selected molecular orbitals of the complexes **3**, **4a-c** and their compositions in singlet and triplet state, where L = μ-bpy-2H ligand, L′ = X (Halide or CF_3COO ligands) and L″ = PPh_3 ligand.

		Complex 3					**Complex 4a**				
		Energy	Components(%)				Energy	Components(%)			
State	MO	(eV)	Pt	L	L′	L″	(eV)	Pt	L	L′	L″
Singlet	LUMO+5	-1.117	8	2	1	89	-1.108	5	4	1	90
	LUMO+4	-1.130	3	2	0	95	-1.116	4	2	0	94
	LUMO+3	-1.160	28	13	2	58	-1.137	30	12	3	55
	LUMO+2	-1.428	35	16	3	46	-1.381	12	66	1	21
	LUMO+1	-1.445	14	63	1	22	-1.441	34	18	6	43
	LUMO	-2.086	4	89	0	7	-2.021	4	88	1	7
	HOMO	-6.120	45	53	3	1	-5.904	44	38	18	1
	HOMO-1	-6.425	81	3	9	7	-6.330	57	13	29	1
	HOMO-2	-6.454	78	4	8	9	-6.446	87	5	0	8
	HOMO-3	-6.633	70	23	5	1	-6.461	79	5	3	13
	HOMO-4	-6.935	8	7	7	78	-6.643	16	5	53	26
	HOMO-5	-6.940	11	5	7	76	-6.655	23	5	56	16
		Complex 4b					**Complex 4c**				
		Energy	Components(%)				Energy	Components(%)			
State	MO	(eV)	Pt	L	L′	L″	(eV)	Pt	L	L′	L″
Singlet	LUMO+5	-1.114	9	3	0	88	-1.139	6	4	0	90
	LUMO+4	-1.119	10	2	0	88	-1.145	5	2	0	93
	LUMO+3	-1.157	27	12	4	56	-1.321	31	15	1	47
	LUMO+2	-1.373	9	66	1	24	-1.449	12	67	1	19
	LUMO+1	-1.474	29	18	6	47	-1.675	33	20	8	39
	LUMO	-2.007	3	89	1	7	-2.084	5	88	1	7
	HOMO	-5.827	41	31	28	1	-5.832	36	25	38	1
	HOMO-1	-6.185	22	9	46	23	-6.046	9	6	77	8
	HOMO-2	-6.286	9	5	67	19	-6.053	9	5	77	9
	HOMO-3	-6.310	7	5	69	18	-6.085	30	6	63	2
	HOMO-4	-6.432	44	5	1	50	-6.447	83	8	3	6
	HOMO-5	-6.472	41	6	4	48	-6.477	77	11	3	9

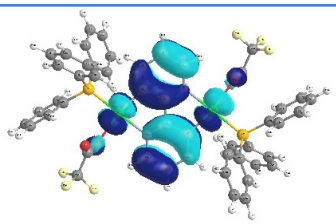	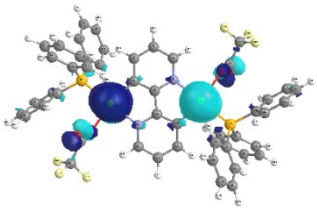	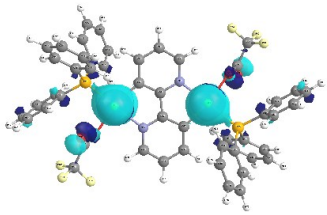
HOMO (-6.120 eV)	**HOMO-1 (-6.425 eV)**	**HOMO-2 (-6.454 eV)**
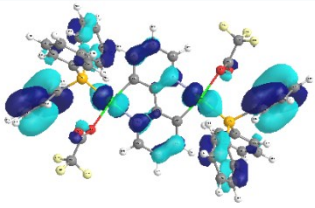	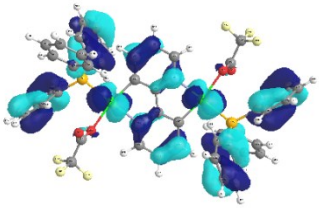	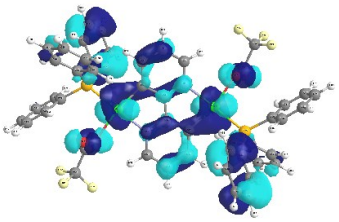
HOMO-6 (-7.031 eV)	**HOMO-8 (-7.067 eV)**	**HOMO-12 (-7.193 eV)**
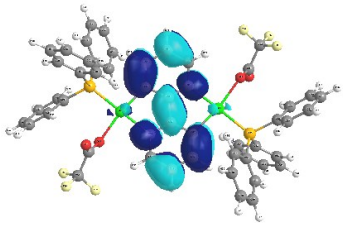	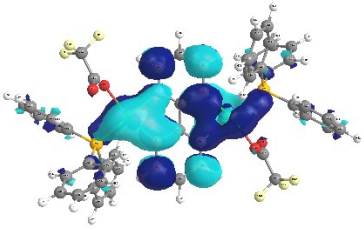	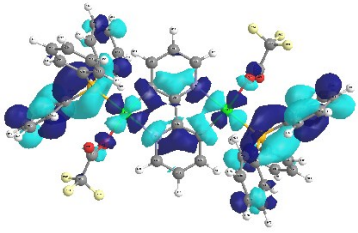
LUMO (-2.086 eV)	**LUMO+1 (-1.445 eV)**	**LUMO+2 (-1.428 eV)**
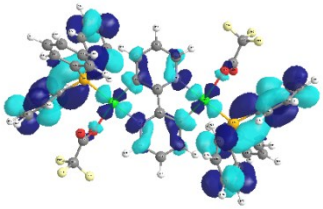	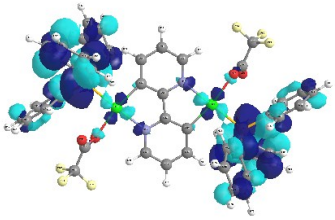	
LUMO+3 (-1.160 eV)	**LUMO+5 (-1.117 eV)**	

Figure S12. MO plots of the complex **3**.

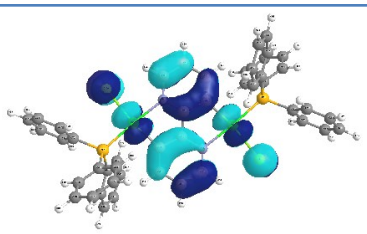	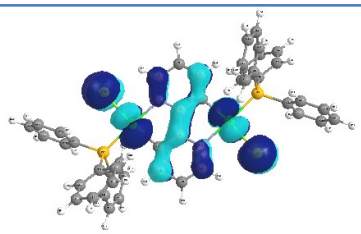	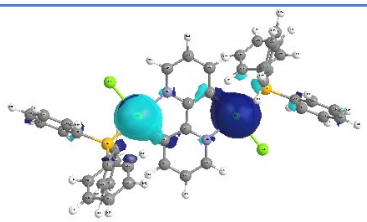
HOMO (-5.904 eV)	**HOMO-1 (-6.330 eV)**	**HOMO-2 (-6.446 eV)**
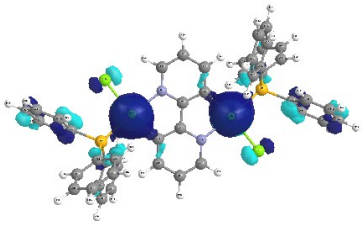	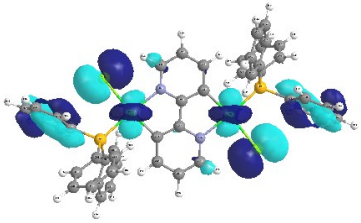	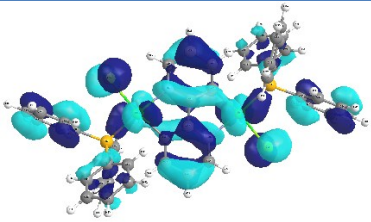
HOMO-3 (-6.461 eV)	**HOMO-5 (-6.655 eV)**	**HOMO-6 (-6.911 eV)**
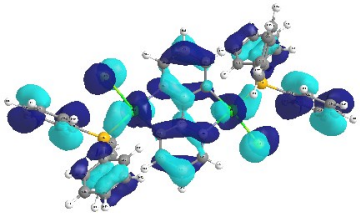	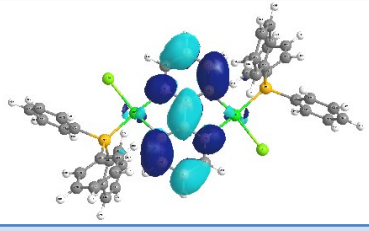	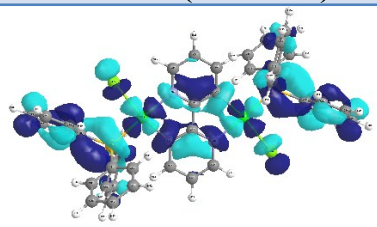
HOMO-7 (-6.927 eV)	**LUMO (-2.021 eV)**	**LUMO+1 (-1.441 eV)**
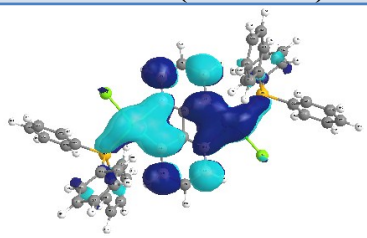	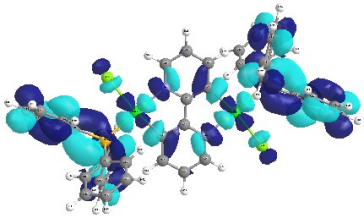	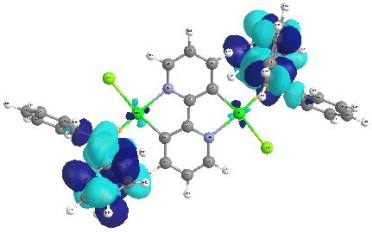
LUMO+2 (-1.381 eV)	**LUMO+3 (-1.137 eV)**	**LUMO+4 (-1.116 eV)**

Figure S13. MO plots of the complex **4a**.

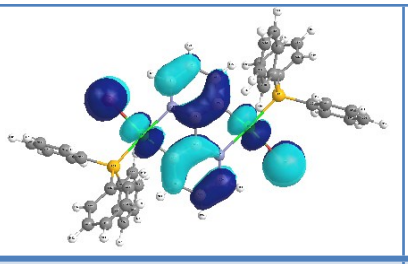	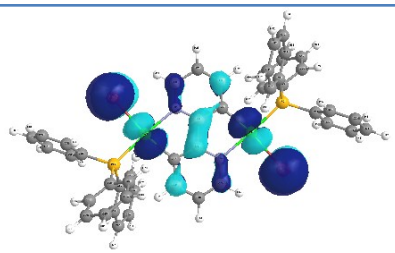	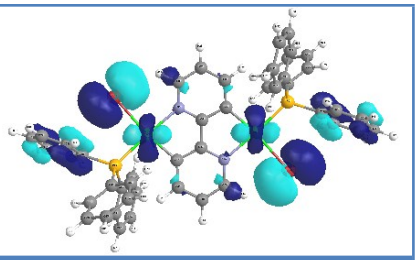
HOMO (-5.827 eV)	**HOMO-1 (-6.185 eV)**	**HOMO-2 (-6.286 eV)**
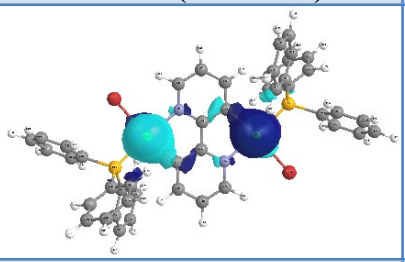	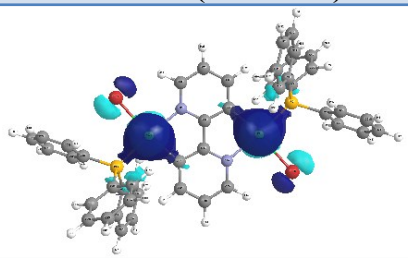	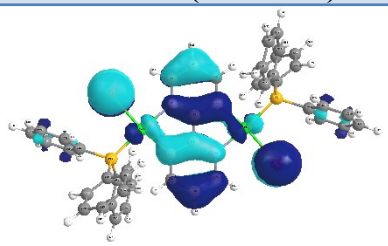
HOMO-4 (-6.432 eV)	**HOMO-5 (-6.472 eV)**	**HOMO-6 (-6.760 eV)**
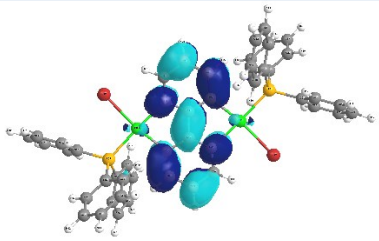	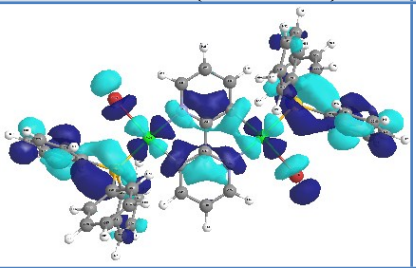	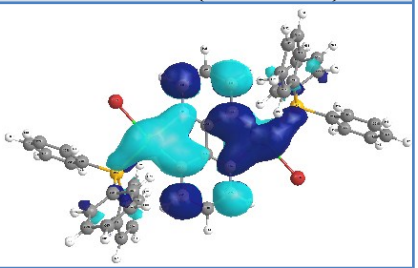
LUMO (-2.007 eV)	**LUMO+1 (-1.474 eV)**	**LUMO+2 (-1.373 eV)**
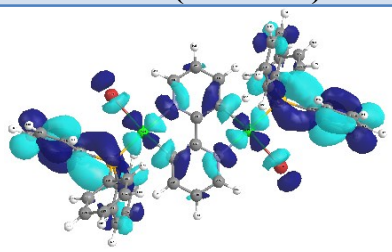	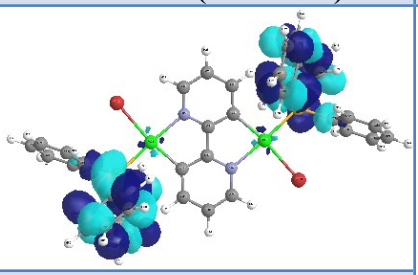	
LUMO+3 (-1.157 eV)	**LUMO+4 (-1.119 eV)**	

Figure S14. MO plots of the complex **4b**.

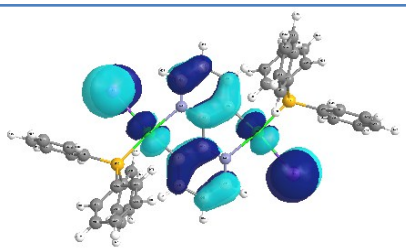	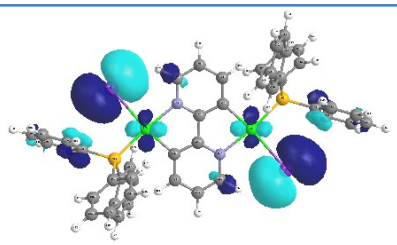	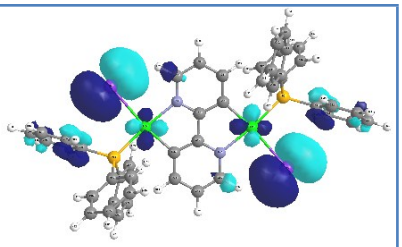
HOMO (-5.832 eV)	**HOMO-1 (-6.046 eV)**	**HOMO-2 (-6.053 eV)**
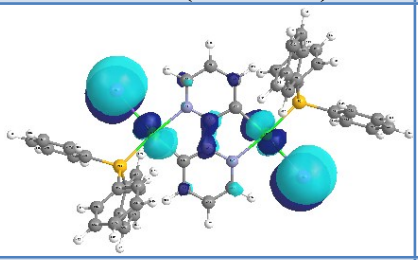	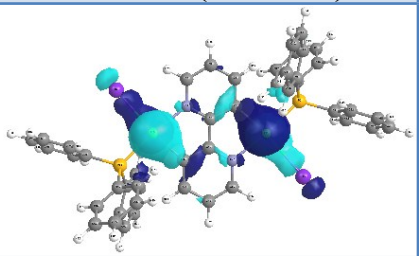	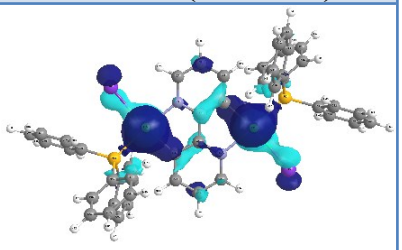
HOMO-3 (-6.085 eV)	**HOMO-4 (-6.447 eV)**	**HOMO-5 (-6.477 eV)**
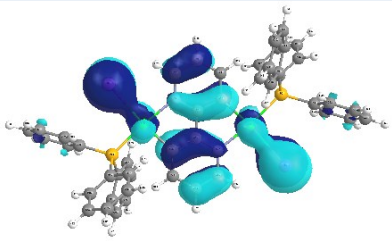	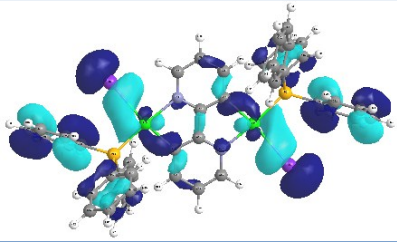	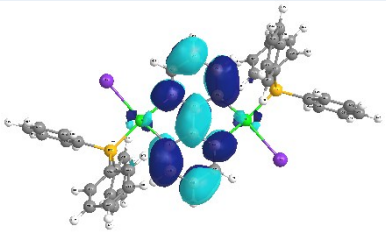
HOMO-6 (-6.594 eV)	**HOMO-8 (-6.871 eV)**	**LUMO (-2.084 eV)**
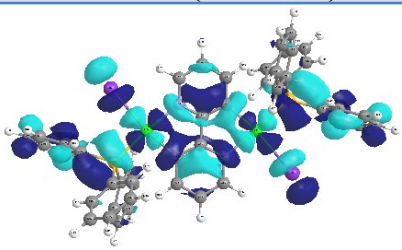	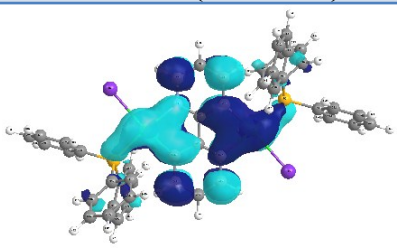	
LUMO+1 (-1.675 eV)	**LUMO+2 (-1.449 eV)**	

Figure S15. MO plots of the complex **4c**.

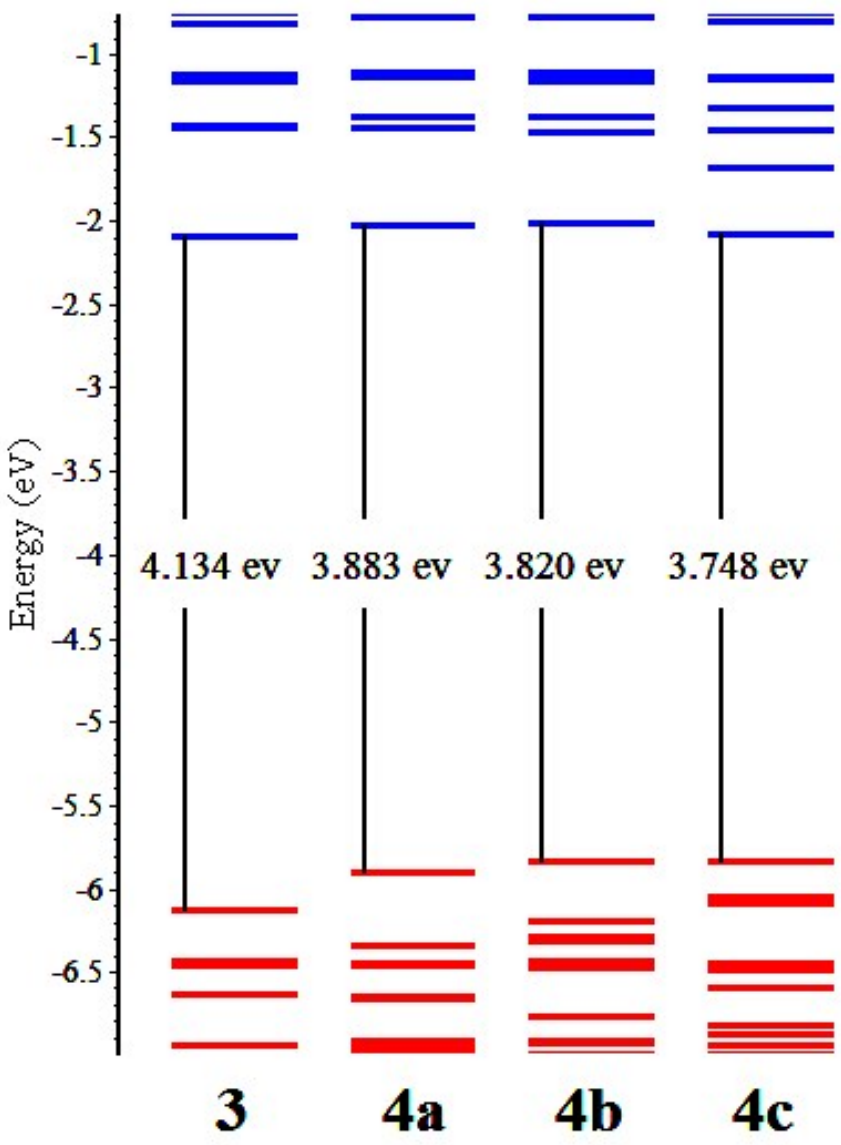

Figure S16. Comparative energy levels diagram for the calculated MOs of complexes **3**, **4a-c**.

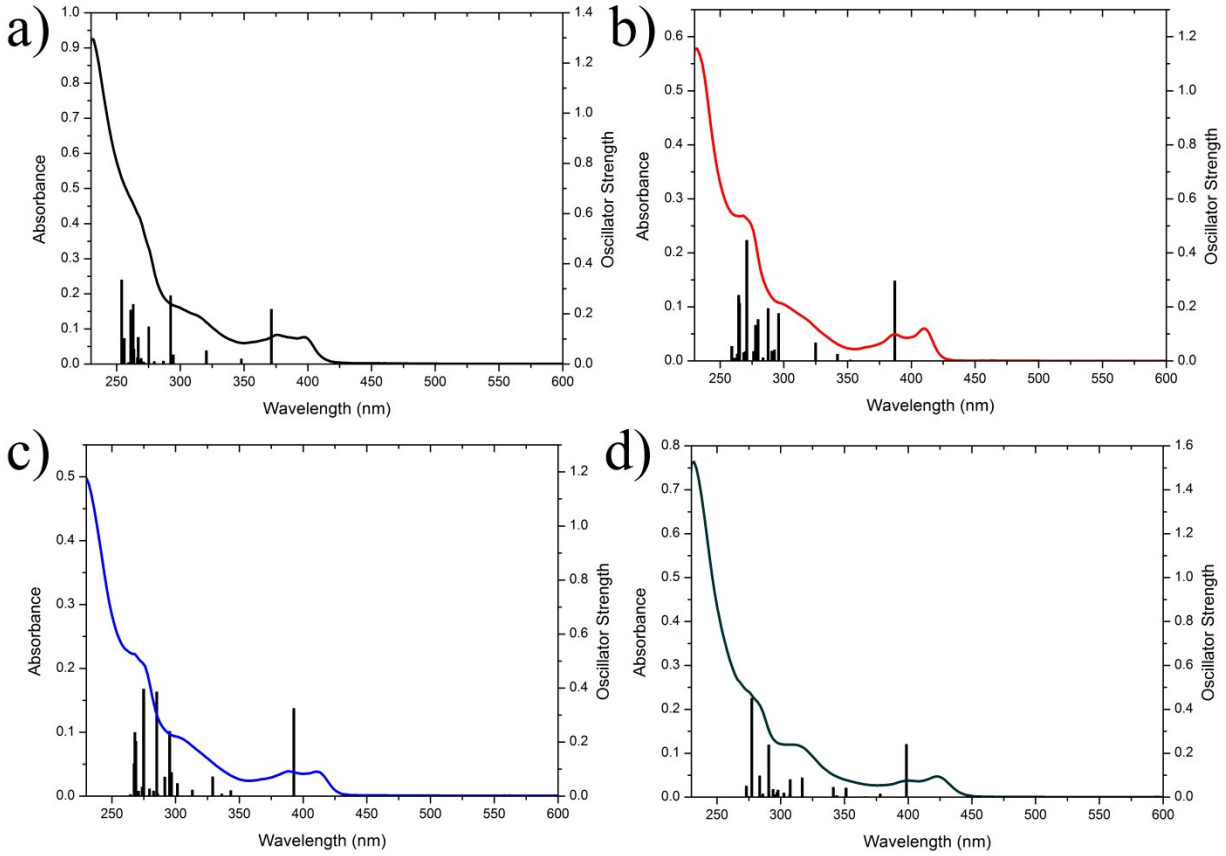

Figure S17. Overlaid experimental absorbance spectra and calculated TD-DFT bars for a) **3**, b) **4a**, c) **4b** and d) **4c**.

Table S7. Wavelengths and corresponding nature of transitions for the complexes **3**, **4a-c** where L = μ-bpy-2H ligand, L′ = X (Halide or CF_3COO ligands) and L″ = PPh_3 ligand.

Complex	Calculated λ (nm)(*f*)	Transitions(Contribution)	Assignment
3	371 (0.156)	HOMO→LUMO (0.69)	ILCT/MLCT
	347 (0.015)	HOMO-2→LUMO (0.69)	MLCT/L′LCT
	320 (0.038)	HOMO-2→LUMO+2 (0.55)	MLCT/ML″CT/L′MCT
		HOMO-1→LUMO+3 (0.28)	MLCT/ML″CT/L′MCT
		HOMO-1→LUMO+5 (0.16)	ML″CT/L′L″CT
	294 (0.027)	HOMO-1→LUMO+1 (0.66)	MLCT/L′MCT
	292 (0.195)	HOMO-8→LUMO (0.48)	L″LCT/ILCT/MLCT
		HOMO-6→LUMO (0.41)	L″MCT/ILCT/MLCT
		HOMO-12→LUMO (0.19)	ILCT/L″MCT/MLCT/L′MCT
4a	387 (0.148)	HOMO→LUMO (0.69)	ILCT/MLCT/L′LCT
	342 (0.013)	HOMO-3→LUMO (0.68)	MLCT/L′LCT
		HOMO-5→LUMO (0.10)	L′LCT/L″LCT/MLCT
	324 (0.034)	HOMO-3→LUMO+1 (0.54)	MLCT/ML″CT
		HOMO-2→LUMO+3 (0.31)	MLCT/ML″CT
		HOMO-2→LUMO+4 (0.13)	ML″CT
	295 (0.088)	HOMO-6→LUMO (0.48)	ILCT/L″LCT/MLCT/L′LCT
		HOMO-7→LUMO (0.31)	ILCT/L″LCT/MLCT/L′LCT
		HOMO-1→LUMO+2 (0.26)	ILCT/L′LCT/L′MCT/ML″CT
4b	392 (0.137)	HOMO→LUMO (0.69)	ILCT/MLCT/L′LCT
	343 (0.009)	HOMO-5→LUMO (0.49)	MLCT/L′LCT
		HOMO-2→LUMO (0.49)	MLCT/L′LCT/L″LCT
	329 (0.030)	HOMO-5→LUMO+1 (0.53)	MLCT/ML″CT
		HOMO-4→LUMO+3 (0.34)	ML″CT/MLCT
		HOMO-2→LUMO+1 (0.18)	L′LCT/L′L″CT/MLCT/ML″CT
	301 (0.020)	HOMO-6→LUMO (0.57)	ILCT/L′LCT/MLCT
		HOMO-1→LUMO+2 (0.33)	L′LCT/ILCT/MLCT
	296 (0.037)	HOMO→LUMO+4 (0.58)	L′L″CT/LL″CT/ML″CT
		HOMO-1→LUMO+2 (0.29)	L′LCT/ILCT/MLCT
		HOMO-6→LUMO (0.16)	ILCT/L′LCT/MLCT
	295 (0.101)	HOMO-1→LUMO+2 (0.52)	L′LCT/ILCT/MLCT
		HOMO-6→LUMO (0.25)	ILCT/L′LCT/MLCT
		HOMO-1→LUMO+4 (0.13)	L′L″CT/LL″CT/ML″CT
4c	398 (0.120)	HOMO→LUMO (0.69)	ILCT/MLCT/L′LCT
	351 (0.021)	HOMO-5→LUMO (0.47)	MLCT/L′LCT

	HOMO-5→LUMO+1 (0.38)	MLCT/ML″CT
	HOMO-1→LUMO+1 (0.11)	L′MCT/L′LCT/L′L″CT
341 (0.022)	HOMO-1→LUMO+1 (0.39)	L′MCT/L′LCT/L′L″CT
	HOMO-5→LUMO+1 (0.34)	MLCT/ML″CT
	HOMO-5→LUMO (0.32)	MLCT/L′LCT
316 (0.044)	HOMO-6→LUMO (0.66)	ILCT/L′LCT/MLCT
	HOMO-5→LUMO (0.12)	MLCT/L′LCT
307 (0.040)	HOMO-3→LUMO+2 (0.55)	L′MCT/L′LCT/L′L″CT
	HOMO-2→LUMO+2 (0.37)	L′MCT/L′LCT/L′L″CT
293 (0.018)	HOMO-4→LUMO+2 (0.51)	L′MCT/L′LCT/L′L″CT/MLCT
	HOMO-8→LUMO (0.26)	L′LCT/L″LCT/MLCT

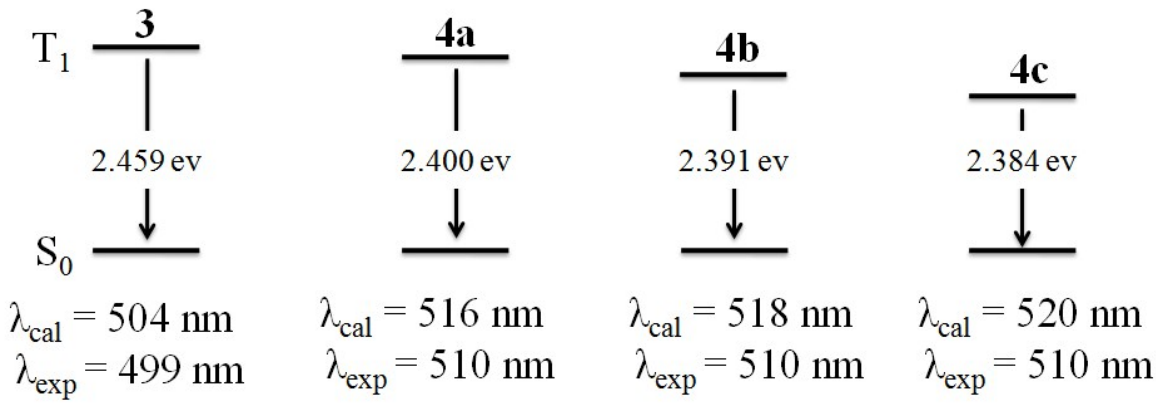

Figure S18. The comparative $T_1 \rightarrow S_0$ energy gaps diagram, and comparison between the calculated emission wavelengths and their corresponding experimental values for all the complexes.

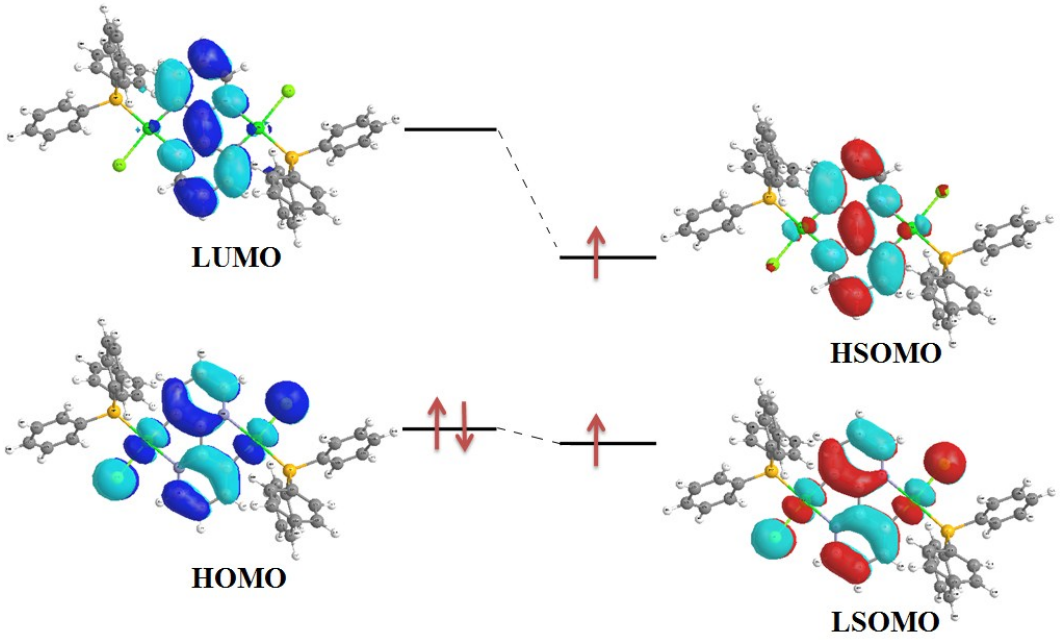

Figure S19. Molecular orbital plots for the computed S_0 (Left) and T_1 (Right) states of complex **4a**.

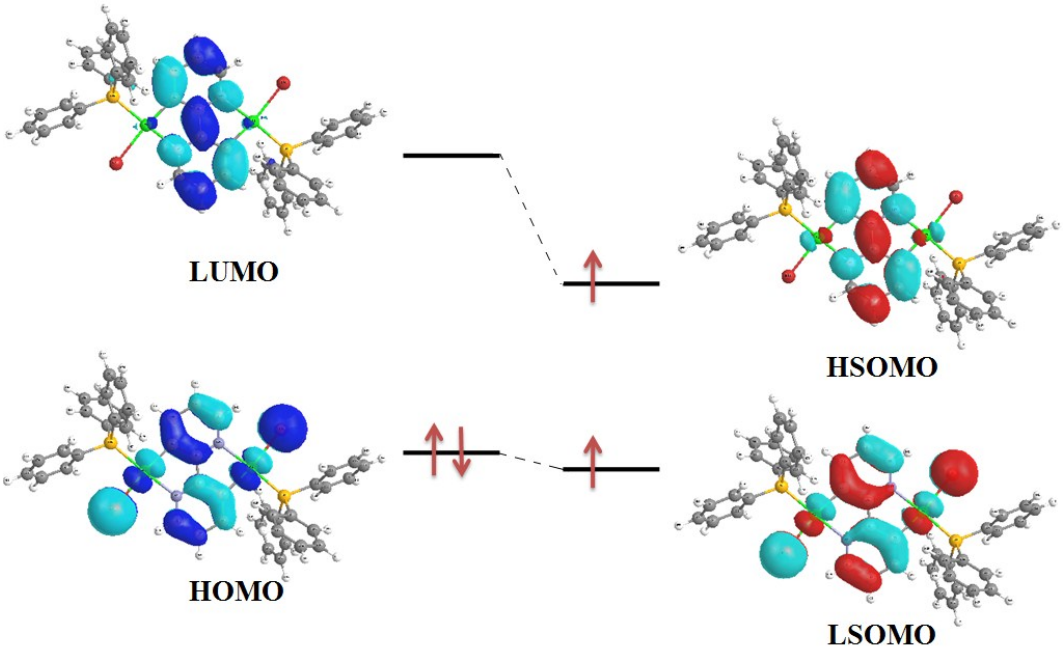

Figure S20. Molecular orbital plots for the computed S_0 (Left) and T_1 (Right) states of complex **4b**.

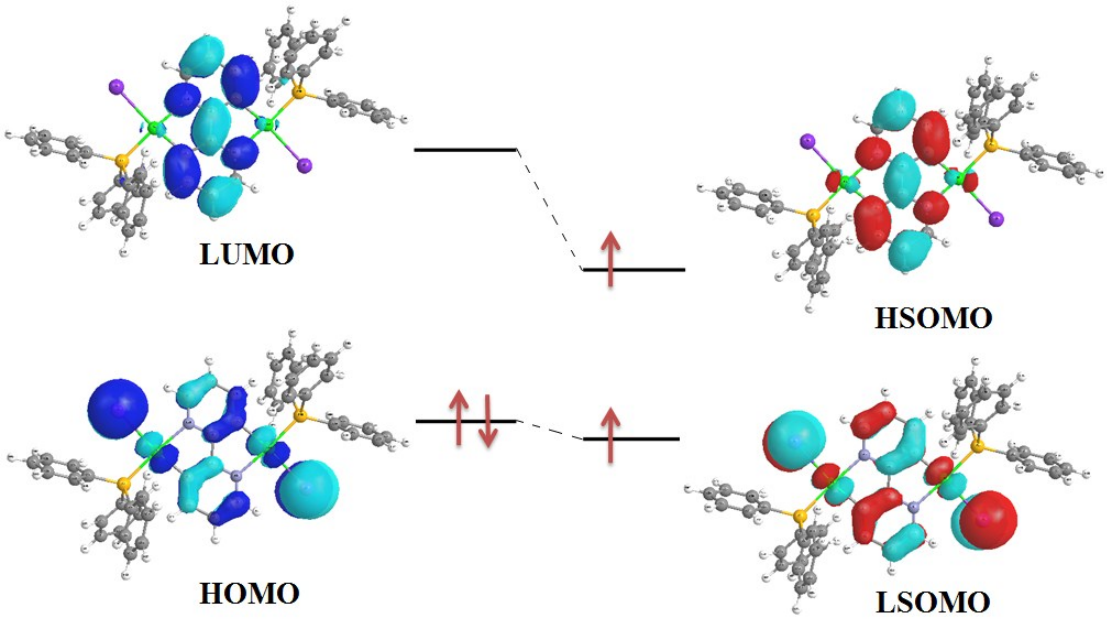

Figure S21. Molecular orbital plots for the computed S_0 (Left) and T_1 (Right) states of complex **4c**.

Table S8. Crystallographic and structure refinement data for the complex **3**.

Crystallographic Data	**Complex 3**
Formula	$C_{50}\ H_{36}\ F_6\ N_2\ O_4\ P_2\ Pt_2$
Formula Weight	1294.91
Crystal System	triclinic
Space group	$P\bar{1}$
a, b, c [Angstrom]	9.3123(19) 10.147(2) 16.201(3)
alpha, beta, gamma [deg]	83.79(3) 76.06(3) 67.55(3)
V [Ang**3]	1373.0(6)
Z	1
D(calc) [g/cm**3]	1.670
Mu(MoKa) [/mm]	5.212
M_r	1381.13
F(000)	672
h, k, l max	10, 11, 19
Crystal Size [mm]	0.20 × 0.10 × 0.10
Temperature (K)	293
Radiation [Angstrom]	MoKα, 0.71073
Theta Min-Max [Deg]	2.4, 24.7
Dataset	-11: 11 ; -12: 11 ; -18: 19
Tot., Uniq. Data, R(int)	9987, 4792, 0.056
Observed Data [I > 2.0 sigma(I)]	3615
Nref, Npar	4622, 299
R, wR2, S	0.0326, 0.0696, 0.849
$w=1/[\sigma^2(Fo^2)+(0.0319P)^2]$ where $P=(Fo^2+2Fc^2)/3$	
Max. and Av. Shift/Error	0.00, 0.00
Data completeness	0.992